ARTICLE IN PRESS

Journal of Engineering Research xxx (xxxx) xxx

Contents lists available at ScienceDirect

Journal of Engineering Research

journal homepage: www.journals.elsevier.com/journal-of-engineering-research

Full length article

Multi-sensor thermo–electro–mechanical characterization of an SMA wire for wearable actuation design

Q.Y. Hamid [a,b], W.Z. Wan Hasan [c,d,*], M.A. Azmah Hanim [a,e], A.A. Nuraini [a], M.N. Hamidon [c,f]

[a] Department of Mechanical and Masnufacturing Engineering, Faculty of Engineering, Universiti Putra Malaysia, Serdang, Selangor 43400, Malaysia
[b] Department of Power Mechanic Techniques Engineering, Engineering Technical College of Mosul, Northern Technical University, Mosul 41001, Iraq
[c] Department of Electrical and Electronic Engineering, Faculty of Engineering, Universiti Putra Malaysia, Serdang, Selangor 43400, Malaysia
[d] Advanced Lightning, Power and Energy Research (ALPER), Universiti Putra Malaysia, Serdang 43400, Malaysia
[e] Advanced Engineering Materials and Composites Research Center (AEMC), Faculty of Engineering, Universiti Putra Malaysia, Serdang, Selangor 43400, Malaysia
[f] Institute of Nanoscience and Nanotechnology (ION2), Universiti Putra Malaysia, Serdang 43400, Malaysia

A R T I C L E I N F O

Keywords:
SMA
Arduino
PWM
Wearable robotics
Actuators

A B S T R A C T

Shape Memory Alloy (SMA) wires are widely used in wearable and soft-robotic systems due to their high power-to-weight ratio and muscle-like behavior. However, their strong thermo-electro-mechanical coupling requires precise experimental characterization to ensure safe and efficient operation. This study presents an Arduino-based multi-sensor platform for characterizing a 0.38 mm Flexinol® NiTi SMA wire under controlled electrical actuation. The system integrates non-contact infrared temperature sensing (MLX90614-BCC), force measurement using a load cell with HX711, displacement monitoring via VL6180X time-of-flight sensor, and real-time electrical tracking using ACS712 current and voltage modules. Regulated current pulses and PWM-controlled Joule heating were applied following a defined protocol, with prior calibration to ensure accuracy. Results demonstrate the transient thermal response, force–time behavior, stroke characteristics, and electrical input profiles under varying conditions. The synchronized multi-parameter acquisition identifies safe operating windows for wearable rehabilitation applications and provides a scalable framework for optimizing SMA-driven robotic systems.

Introduction

Intelligent materials—including ionic polymer–metal composites (IPMCs), dielectric elastomers (DEAs), piezoelectric polymers (PEPs), composite materials, and shape memory alloys (SMAs) exhibit adaptive responses to external stimuli and provide diverse functional advantages. Consequently, these materials have been increasingly applied in life-related fields, particularly wearable robotics and biomedical applications, where compactness, compliance, and safe human machine interaction are essential [1–11]. Shape memory alloys (SMAs) constitute a unique class of smart materials capable of generating large recoverable strains through reversible martensite–austenite phase transformations triggered by thermal or electrical stimuli [12–14]. Among these materials, nickel–titanium (NiTi) alloys have received considerable attention due to their high power-to-weight ratio, compact form factor, silent operation, and muscle-like actuation behavior [1,15–18]. These characteristics make SMA wire actuators particularly attractive for wearable robotics, soft robotic systems, and rehabilitation devices, where lightweight, compliant, and biomimetic actuation is essential for safe and effective human–machine interaction [19–24].

In electrically driven SMA actuators, axial contraction and force generation are achieved through Joule heating, which induces the martensite-to-austenite phase transformation. Upon removal of the electrical input, the actuator cools and returns to its original shape through the reverse transformation, typically assisted by an external bias load or elastic element [13,25]. This strongly coupled thermo–electro–mechanical behavior enables simple actuator architectures but also introduces significant challenges in control and performance repeatability. The dynamic response of SMA wires is highly sensitive to electrical current amplitude, heating duration, wire geometry, and heat

* Corresponding author at: Department of Electrical and Electronic Engineering, Faculty of Engineering, Universiti Putra Malaysia, Serdang, Selangor 43400, Malaysia

E-mail addresses: gs60418@student.upm.edu.my, qussay.hamid@ntu.edu.iq (Q.Y. Hamid), wanzuha@upm.edu.my (W.Z.W. Hasan), azmah@upm.edu.my (M.A.A. Hanim), nuraini@upm.edu.my (A.A. Nuraini), mnh@upm.edu.my (M.N. Hamidon).

https://doi.org/10.1016/j.jer.2026.07.013
Received 24 February 2026; Received in revised form 5 July 2026; Accepted 20 July 2026
Available online 20 July 2026

Please cite this article as: Q.Y. Hamid et al., *Journal of Engineering Research,* https://doi.org/10.1016/j.jer.2026.07.013

dissipation conditions, particularly under transient actuation cycles [26,27].

A major limitation in the practical deployment of SMA wire actuators, especially in wearable and rehabilitation applications, is their thermal behavior. Slow cooling rates restrict actuation frequency and responsiveness, while excessive temperature rise can lead to material degradation, reduced fatigue life, and potential safety concerns when operating near the human body [28–31]. Consequently, understanding and accurately characterizing the thermal and electrical response of SMA wires under realistic operating conditions is critical for defining safe actuation windows and optimizing performance [32].

Previous studies have shown that SMA actuator performance is strongly influenced by alloy composition, transformation temperature, and wire diameter [17,33–35]. Low-transformation-temperature (LT) NiTi alloys are generally preferred for biomedical and wearable systems because they operate at lower activation temperatures, reducing power consumption and thermal risk compared to high-temperature SMAs [36–38]. Commercial Flexinol® NiTi wires with diameters in the range of 0.30–0.50 mm have therefore been widely adopted in hand rehabilitation and soft robotic devices due to their favorable balance between force output, displacement capability, and thermal response [1,39,40]. Wires with diameters around 0.38 mm are frequently reported to provide sufficient force for hand-assistive tasks—typically on the order of 15–20 N—without excessive electrical demand or prolonged cooling times [17,41].

While numerical and analytical models have been extensively used to estimate the thermal and mechanical behavior of SMA wires, their predictive accuracy is often limited by simplifying assumptions related to convective cooling, temperature-dependent material properties, and phase transformation hysteresis [42–44]. As a result, experimental characterization remains essential to capture the true transient behavior of SMA actuators and to establish reliable correlations between electrical excitation, temperature evolution, contraction displacement, and generated force. To provide a comprehensive overview of existing studies, representative SMA characterization platforms and wearable rehabilitation systems are compared in Table 1. The comparison highlights the measured physical variables, control and data-acquisition platforms, and the primary focus or limitations of each study, thereby identifying the research gap addressed by the proposed characterization platform.

As summarized in Table 1, previous studies have mainly focused either on SMA actuator characterization or on wearable rehabilitation applications. Actuator characterization studies generally investigated selected thermal, mechanical, or electrical variables, whereas wearable rehabilitation systems primarily emphasized device design, motion control, and functional evaluation. Although several studies reported temperature, force, displacement, current, or voltage measurements, synchronized acquisition of all five parameters under multiple current-duration operating conditions remains limited. Moreover, many existing characterization systems rely on laboratory-grade instrumentation, while wearable systems often lack detailed actuator-level thermo-electro-mechanical evaluation. This gap highlights the need for a low-cost, portable, and expandable experimental platform that can characterize SMA actuators while supporting future integration into wearable rehabilitation devices [11,38,45–55].

To address this gap, the present study develops a synchronized thermo-electro-mechanical characterization platform capable of simultaneously measuring temperature, force, displacement, current, and voltage under multiple operating conditions. Unlike conventional SMA characterization platforms that typically evaluate only selected thermal, electrical, or mechanical variables, the proposed system integrates all five measurements within a single synchronized experimental framework to identify practical operating windows for electrically driven SMA actuators used in wearable rehabilitation. The platform is implemented

Table 1
Comparison of representative SMA characterization and wearable rehabilitation systems.

Year/ Ref.	Primary Application	T	F	x	I	V	Controller / DAQ	Primary Focus / Limitation
2014 [45]	Actuator characterization and control	✓	✓	✓	✓	✓	NI-DAQ + MATLAB	Control-oriented characterization of a single SMA actuator.
2015 [46]	Actuator characterization	✓	✓	✓	×	×	Custom measurement system	Thermo-mechanical characterization without simultaneous electrical measurements.
2017 [47]	Linear actuator characterization	✓	×	✓	✓	✓	Arduino + MATLAB	Thermo-mechanical characterization; force measurement was not included.
2018 [48]	Hand rehabilitation glove	×	✓	✓	✓	×	Arduino Uno	Wearable glove validation without comprehensive actuator characterization.
2018 [49]	Wrist rehabilitation exoskeleton	×	×	✓	✓	×	STM32	Wearable exoskeleton emphasizing control performance.
2018 [38]	Hand rehabilitation glove	×	✓	✓	✓	×	Arduino Mega 2560	Wearable glove with position and force control.
2019 [50]	Smart textile actuator	×	×	✓	×	✓	NI USB−6009 + MATLAB	Mechanical optimization of tube-guided SMA actuators.
2020 [51]	Prosthetic hand	×	✓	✓	✓	✓	Arduino Uno	Application-oriented prosthetic hand validation.
2021 [52]	Soft robotic hand	✓	✓	✓	△	×	DAQ + Pyboard	Characterization of coiled SMA actuators; electrical characterization was incomplete.
2021 [11]	Hand rehabilitation device	△	✓	✓	✓	✓	PWM controller	Development and evaluation of an SMA-driven hand rehabilitation device.
2022 [53]	Actuator characterization	✓	✓	✓	×	×	LabVIEW + DAQ	Thermomechanical characterization using thermal activation rather than electrical excitation.
2023 [54]	Elbow rehabilitation exoskeleton	✓	×	✓	×	△	STM32 + PWM	Motion-control-oriented SMA elbow exoskeleton.
2024 [55]	Soft wearable rehabilitation exoglove	✓	✓	✓	×	×	Arduino Mega 2560	Knitted-SMA exoglove emphasizing ROM, grip force, wearability, and user evaluation.
2025 [11]	SMA spring actuator	✓	✓	✓	✓	×	HBM Quantum + programmable power supply	Fast SMA spring characterization under high-current activation and sub-second response optimization.
This study	Thermo-electro-mechanical characterization platform for wearable rehabilitation	✓	✓	✓	✓	✓	Arduino Mega 2560 + synchronized multi-sensor platform	Low-cost synchronized measurement of temperature, force, displacement, current, and voltage under multiple current-duration operating conditions.

T: Temperature, F: Force, x: Stroke displacement, I: Current, V: Voltage.
Legend: ✓ = experimentally measured/reported; × = not reported; Δ = partially reported or indirectly evaluated.

using a low-cost Arduino Mega 2560 controller integrated with commercially available sensors, providing a cost-effective, modular solution with real-time visualization and automatic data logging on a laptop for subsequent analysis. Furthermore, its modular hardware architecture facilitates straightforward system expansion and provides the synchronized feedback signals required to support the future implementation of closed-loop control strategies and wearable rehabilitation applications.

In this work, an experimental thermo–electro–mechanical characterization of a low-temperature Flexinol® NiTi SMA wire with a diameter of 0.38 mm and a length of 300 mm is presented. An Arduino-based multi-sensor platform was developed to enable synchronized real-time measurement of electrical current and voltage, surface temperature, contraction displacement, and generated actuation force during controlled heating–cooling cycles. The SMA actuator was investigated under three distinct heating durations (1 s, 2 s, and 3 s), selected to represent a broad range of motion demands encountered in rehabilitation exercises, spanning rapid, high-response movements to slower, controlled, and repetitive actuation patterns [56–58]. By systematically evaluating the SMA response across different current levels and activation times, this study provides validated performance data, identifies practical operating limits, and delivers experimentally grounded insight to support the design and optimization of SMA-driven wearable and rehabilitation systems.

Materials and methods

An experimental platform was designed and constructed to characterize the thermo-electro-mechanical behavior of a Shape Memory Alloy (SMA) wire actuator under controlled electrical excitation [46]. The system enables synchronized, real-time measurement of electrical input (current and voltage), surface temperature, axial contraction displacement, and generated force during repeated heating–cooling cycles. The tested actuator was a low-transformation-temperature (LT) Flexinol® nickel–titanium (NiTi) wire with a circular cross-section diameter of 0.38 mm (≈375 μm) and an active length of 300 mm. The wire, composed of approximately 50% nickel and 50% titanium, was supplied by Dynalloy Inc. (Irvine, CA, USA) and used in its straight configuration [26]. The schematic mechanical configuration of the SMA wire actuation rig is illustrated in Fig. 1, while the complete experimental setup is shown in Fig. 2.

The SMA wire was mounted horizontally with one end rigidly fixed to a stationary support and the other end connected to a low friction sliding carriage. A bias spring was aligned in series with a load cell to provide recovery force during cooling and to enable direct measurement of the contraction force generated by the SMA wire [52]. Electrical actuation was achieved through Joule heating using a regulated DC power supply and a metal–oxide–semiconductor field-effect transistor (MOSFET) switching module controlled by an Arduino Mega 2560 microcontroller [48,59,60].

Thermal, mechanical, and electrical responses were measured using an integrated multi-sensor arrangement. Surface temperature was monitored using a non-contact infrared sensor (MLX90614) positioned beneath the SMA wire, while axial displacement was measured using a time-of-flight laser distance sensor (VL6180X) aligned with the sliding carriage. Electrical current and voltage supplied to the SMA wire were recorded using a Hall-effect current sensor (ACS712) and a voltage sensor module, respectively. All sensor signals were acquired synchronously by the microcontroller and transmitted to a host computer for real-time visualization and data logging. This configuration ensured accurate temporal alignment among thermal, electrical, and mechanical measurements, enabling reliable characterization of the SMA wire behavior under cyclic actuation..Table 2,3,4

A complete hardware prototype of the proposed thermo-electro-mechanical characterization platform was designed, fabricated, and experimentally validated for SMA actuation and measurement. **To improve the clarity and reproducibility of the proposed characterization platform, the key electrical, control, and protection parameters are summarized in** Tables 2–4.

The summarized parameters define the hardware architecture and operating limits of the proposed characterization platform. The electrical excitation strategy, PWM-based actuation, and selected operating current-duration conditions are described in the following section.

Power supply and electrical actuation protocol

Safe and efficient actuation of the Shape Memory Alloy (SMA) wire was achieved through careful selection of electrical parameters based on manufacturer specifications and electrical resistance calculations. The tested Flexinol® low-temperature NiTi SMA wire had an active length of 300 mm and a nominal electrical resistance of 8.3 Ω/m, resulting in a total resistance of approximately 2.49 Ω. Using Ohm's law, the theoretical actuation voltages corresponding to applied currents of 1.3 A, 1.6 A, and 2.2 A were calculated as 3.24 V, 3.98 V, and 5.48 V, respectively. To account for wiring resistance, connector losses, MOSFET switching drops [59], and the temperature-dependent increase in SMA resistance during heating, an additional voltage margin of approximately 1 V was incorporated. Accordingly, practical power-supply settings of 4.3 V, 5.0 V, and 6.5 V were employed.

Electrical actuation was implemented using a regulated DC power supply with current-limiting capability and a PWM-controlled MOSFET driven by an Arduino Mega 2560 microcontroller. The actuation protocol applied three current-duration combinations, namely 1.3 A for 3 s, 1.6 A for 2 s, and 2.2 A for 1 s, as summarized in Table 5. These operating conditions were selected to provide different electrical heating profiles while ensuring that the SMA wire reached the austenitic transformation range (As ≈ 68 °C to Af ≈ 78 °C), thereby initiating the martensite-to-austenite phase transformation responsible for wire contraction. The high-current short-duration condition (2.2 A–1 s) provides rapid heating and fast actuation, whereas the medium-current

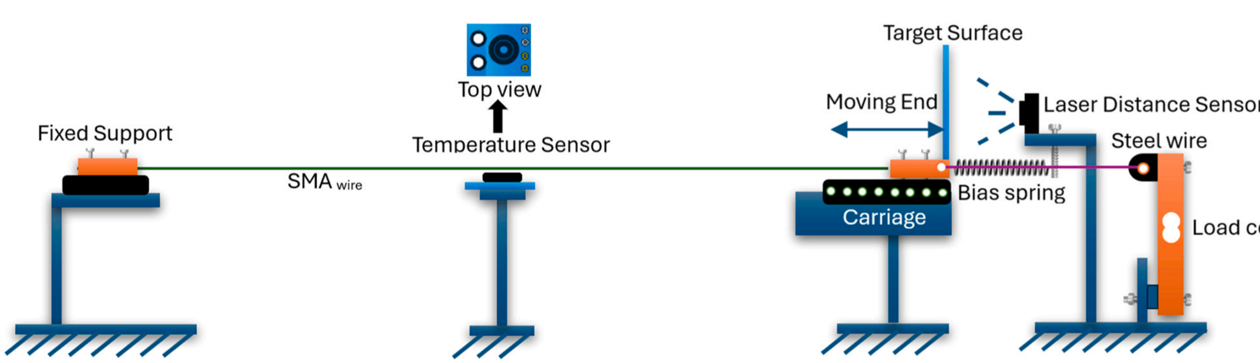

Fig. 1. Schematic of the SMA Wire Actuation Rig and Sensor Arrangement.

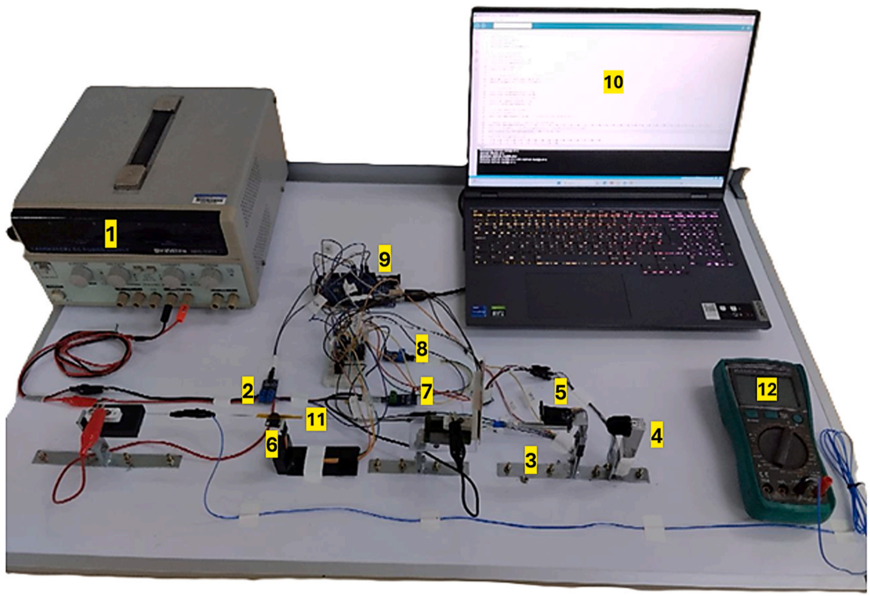

Fig. 2. Experimental setup for SMA actuation and measurement. (1) DC power supply, (2) MOSFET driver module, (3) mechanical frame with SMA wire and bias spring, (4) load cell with HX711 amplifier, (5) laser distance sensor (TOF050C), (6) infrared temperature sensor (MLX90614), (7) current sensor (ACS712), (8) voltage sensor module, (9) Arduino Mega 2560 microcontroller, (10) laptop for data acquisition and control, (11) SMA wire, and (12) digital multimeter for calibration and validation.

Table 2
Electrical parameters of the proposed characterization platform.

Parameter	Value / Specification
SMA actuator	Flexinol® LT NiTi wire
Wire diameter	0.38 mm
Active wire length	300 mm
Material composition	~50% Ni / 50% Ti
Nominal resistance	8.3 Ω/m
Total wire resistance	2.49 Ω
Power supply	Regulated DC power supply
Switching device	MOSFET driver module
Control method	PWM
Current levels	1.3 A, 1.6 A, 2.2 A
Heating durations	3 s, 2 s, 1 s
Theoretical voltages	3.24, 3.98, 5.48 V
Practical supply voltages	4.3, 5.0, 6.5 V

Table 3
Control and data acquisition parameters.

Parameter	Specification
Main controller	Arduino Mega 2560
Temperature sensor	MLX90614 infrared sensor
Force sensor	Load cell + HX711 amplifier
Displacement sensor	VL6180X (TOF050C)
Current sensor	ACS712
Voltage sensor	Voltage sensor module
Host interface	Laptop (serial communication)
Data visualization	Real-time monitoring
Data storage	Automatic logging for post-processing
Measurement mode	Synchronized multi-sensor acquisition

(1.6 A–2 s) and low-current (1.3 A–3 s) conditions provide progressively smoother actuation with reduced thermal loading. Rather than evaluating a single operating point, these three conditions represent a practical range of actuation profiles that support different rehabilitation training scenarios, including rapid grasping, moderate functional movements, and slower controlled therapeutic exercises. Consequently, the proposed platform enables comprehensive evaluation of SMA performance under operating conditions representative of diverse wearable

Table 4
Protection and operating parameters.

Parameter	Specification
Actuation method	PWM-controlled Joule heating
Current limiting	Regulated DC power supply
Voltage margin	~1 V to compensate for wiring/MOSFET losses
Thermal protection	Operating current–time combinations selected to maintain safe thermal operation
Cooling mechanism	Natural air cooling
Safe operating conditions	2.2 A–1 s; 1.6 A–2 s; 1.3 A–3 s
System objective	Stable, repeatable thermo-electro-mechanical characterization

Table 5
Actuation current and duration settings for SMA wire testing.

Current applied	Time (sec)
1.3 A	3 s
1.6 A	2 s
2.2 A	1 s

rehabilitation applications while maintaining safe thermal operation [28].

Pulse-width modulation was employed to regulate the average heating power delivered to the SMA wire, improving energy efficiency and preventing excessive temperature rise by exploiting the SMA's relatively slow thermal response. During each heating–cooling cycle, electrical current and voltage were continuously monitored, allowing instantaneous power ($P = V \cdot I$) and total energy input ($E = V \cdot I \cdot t$) to be quantified. A real-time safety routine immediately interrupted actuation if predefined current or temperature thresholds were exceeded, ensuring safe operation of both the SMA element and the electronic components. All thermal, mechanical, and electrical signals were synchronously acquired at a sampling rate of 10 Hz and streamed in real time to a host computer for data logging and subsequent analysis, enabling comprehensive thermo-electro-mechanical characterization of the SMA actuator under controlled and application-relevant actuation conditions.

Electrical actuation, PWM control, and data acquisition

Electrically driven actuation of the SMA wire was achieved through Joule heating, in which the martensite–austenite phase transformation is governed by the rate of heat transfer to and from the material. Direct current input rapidly raises the SMA temperature to induce contraction, while natural convective cooling enables recovery upon current removal. To regulate the average heating power and enable controlled actuation, pulse-width modulation (PWM) was employed. By varying the duty cycle of the applied signal, PWM allows fine control of the delivered thermal energy, prevents overheating, and improves energy efficiency, taking advantage of the SMA's relatively slow thermal response to achieve uniform and stable temperature evolution. This approach is particularly suitable for wearable and rehabilitation applications, as it enables operation from portable power sources and provides robustness against voltage fluctuations.

The electrical actuation and measurement process was governed by an Arduino Mega 2560 microcontroller, which coordinated both PWM-based control and synchronized data acquisition. A high-power MOSFET driver was used to switch the SMA wire using a PWM signal, with duty cycles typically set to 100% for rapid heating and reduced values (e.g., 80–90%) to moderate heating rates when required. Heating durations of 1–3 s were applied depending on the selected actuation level. During each experiment, the microcontroller initialized all connected sensing modules—including the load-cell amplifier, current and voltage sensors, infrared temperature sensors, and time-of-flight distance sensor—and acquired calibrated measurements in real time. A safety routine continuously monitored electrical current and SMA surface temperature, immediately interrupting actuation if predefined thresholds were exceeded to prevent overheating or electrical overload. All thermal, mechanical, and electrical signals were synchronously sampled at 10 Hz and streamed to a host computer in CSV format for real-time logging and post-processing, enabling reliable and repeatable thermo-electro-mechanical characterization of the SMA actuator under controlled actuation conditions.

The overall logic of the Arduino-based control and data-acquisition program, including system initialization, PWM-driven actuation, real-time safety monitoring, and synchronized sensor sampling, is

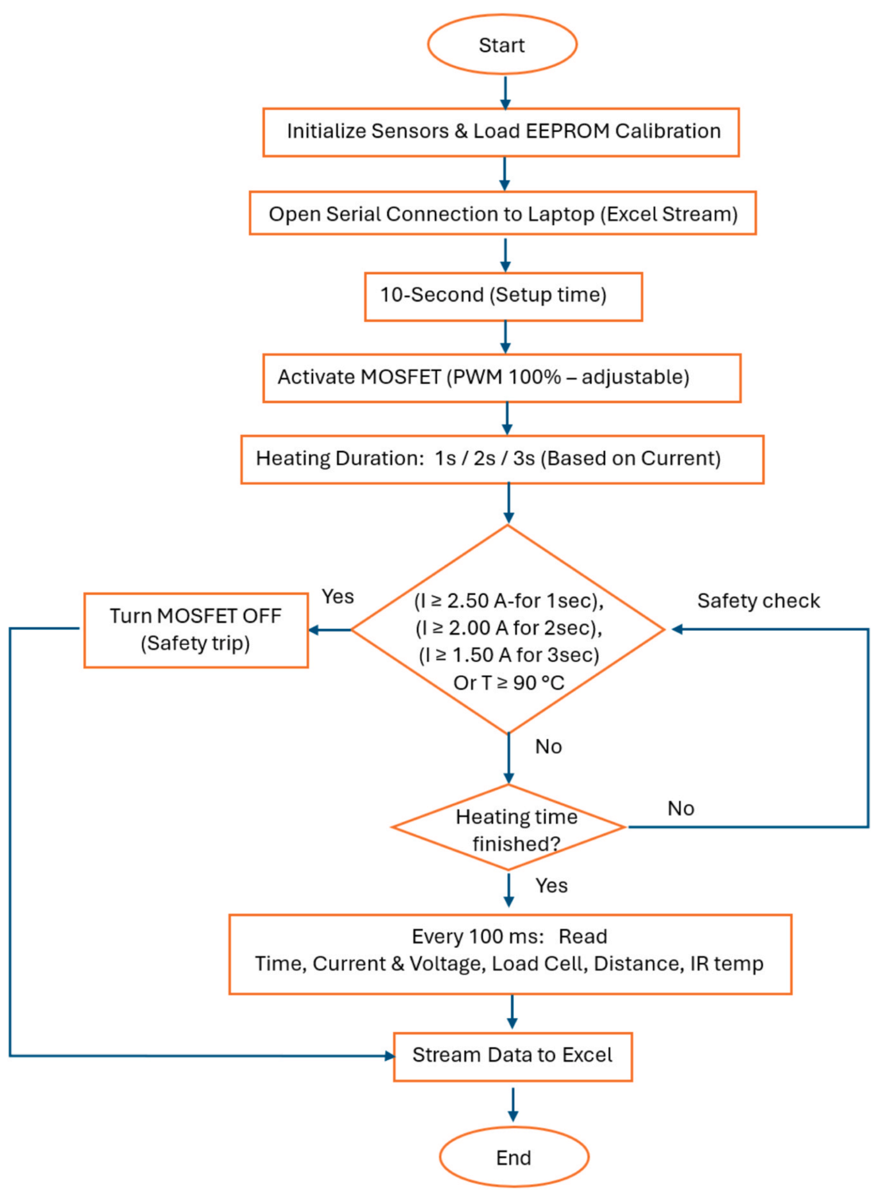

Fig. 3. Arduino-Based SMA Actuation and Data Acquisition Flowchart.

summarized in Fig. 3.

Non-contact temperature measurement using MLX90614-BCC sensor

The surface temperature of the Shape Memory Alloy (SMA) wire was monitored using a non-contact infrared temperature sensor (MLX90614ESF-BCC), positioned approximately 2 cm from the wire to enable real-time temperature measurement during electrical actuation. Initial temperature measurements using a type-K thermocouple electrically insulated with Kapton tape exhibited unstable readings and delayed thermal response, primarily due to poor thermal conduction through the insulation layer and the difficulty of maintaining reliable contact with the electrically active SMA wire. To overcome these limitations, a non-contact infrared sensing approach was adopted, eliminating electrical interference and ensuring consistent temperature acquisition throughout repeated heating–cooling cycles [61].

The BCC variant of the MLX90614 sensor was selected due to its narrow field of view (approximately 10–20°), which is well suited for precise temperature measurement of small-diameter targets such as the 0.38 mm SMA wire used in this study. This focused optical configuration minimizes the influence of surrounding structures and background radiation, which can otherwise distort infrared measurements. In contrast, the standard BAA variant of the MLX90614 features a wide field of view (~90°), making it more appropriate for large surfaces but unsuitable for localized temperature sensing of thin actuators. The narrow spot size and reduced background sensitivity of the MLX90614-BCC enabled accurate and stable monitoring of SMA surface temperature under dynamic actuation conditions, supporting reliable correlation between thermal input and mechanical response [62].

Force measurement using load cell

The force generated by the Shape Memory Alloy (SMA) actuator was measured using a load cell integrated with an HX711 signal-conditioning module. The load cell had a nominal capacity of 5 kg with a resolution of 5 g, providing sufficient sensitivity for capturing the tensile forces produced during SMA contraction. As the SMA wire was electrically heated and contracted, the generated force was transmitted through a series elastic element (bias spring) to the load cell. The spring ensured controlled force transmission and provided a restoring mechanism during the cooling phase, enabling repeatable cyclic actuation [52, 53,63].

The analog output of the load cell was amplified and digitized by the HX711 module and calibrated using known reference masses prior to testing [38]. The measured mass values were converted to force using the standard gravitational relationship:

$$F = m \times g \tag{1}$$

where $F$is the force in newtons, $m$is the measured mass in kilograms, and $g$is the gravitational acceleration (9.81 m·s^{-2}).

The use of a series spring configuration was selected to reflect practical conditions encountered in wearable and rehabilitation systems, where elastic elements are commonly incorporated to improve safety, enhance compliance, and assist actuator recovery. Spring absorbed part of the contraction energy during heating and released it during cooling, reducing residual strain accumulation in the SMA wire and improving repeatability over successive cycles. This configuration enabled stable force measurements while ensuring mechanical protection of the SMA element and consistent recovery behavior, making it suitable for long-term cyclic testing and rehabilitation-oriented actuation studies.

Displacement measurement using VL6180X time-of-flight sensor

The axial contraction displacement of the Shape Memory Alloy (SMA) wire during electrical actuation was measured using a VL6180X time-of-flight (ToF) laser distance sensor positioned directly in front of the moving carriage. To ensure stable and repeatable distance readings, a flat plastic target (50 mm × 50 mm) was rigidly attached to the carriage, providing a uniform reflective surface for the optical measurement. The VL6180X operates by emitting an 850 nm vertical-cavity surface-emitting laser (VCSEL) pulse and determining distance from the photon return time using integrated ToF timing circuitry, enabling direct distance measurement with minimal sensitivity to surface reflectance variations.

The sensor is optimized for short-range measurements (0–60 mm) and exhibits high accuracy in the 10–20 mm range, which closely matches the maximum contraction stroke of the SMA wire (approximately 15 mm). The VL6180X provides a typical resolution of about 1 mm with stable real-time output, making it suitable for continuous displacement tracking during both heating and cooling phases. The sensor was interfaced with the Arduino Mega microcontroller via the I^{2}C communication bus and shared the SDA and SCL lines with other system sensors. Its non-contact operation, compact form factor, and high short-range precision enabled reliable measurement of small-scale SMA displacement throughout repeated actuation cycles.

Electrical signal measurement using current and voltage sensors

The electrical characteristics of the SMA actuation circuit were continuously monitored using a Hall-effect current sensor (ACS712) and a voltage-divider sensing module, enabling real-time measurement of current, voltage, and electrical power supplied to the SMA wire. The ACS712 sensor (5 A range) provided galvanic isolation between the high-current actuation circuit and the Arduino Mega 2560 analog input, ensuring safe operation and reliable signal acquisition. The sensor exhibits a linear sensitivity of approximately 185 mV·A^{-1} , allowing accurate detection of current variations during dynamic heating and cooling cycles. The voltage-sensing module scaled the applied supply voltage (0–25 V range) to the 0–5 V input range of the microcontroller's analog-to-digital converter, enabling direct measurement of the potential difference across the SMA wire [64].

Both current and voltage signals were sampled synchronously with the thermal, force, and displacement measurements at a sampling interval of 100 ms throughout each actuation cycle. Prior to testing, sensor calibration was performed using a precision digital multimeter to correct offset errors and verify linear response. The acquired electrical data were used to compute the instantaneous electrical power delivered to the SMA wire ($P = V \times I$) and the total energy input per actuation cycle ($E = P \times t$). These measurements provided a quantitative basis for correlating electrical input with the resulting thermal response, contraction displacement, and force output of the SMA actuator [65].

Experimental hardware and system integration

The experimental actuation system was built around an Arduino Mega 2560 microcontroller, which coordinated electrical actuation, sensor data acquisition, and serial communication with a host computer. The system integrated multiple sensing modules to enable synchronized monitoring of the SMA wire's thermo-electro-mechanical behavior, including force, displacement, temperature, current, and voltage. Force measurement was performed using a load cell interfaced through an HX711 amplifier [38], while non-contact displacement and temperature measurements were obtained using a VL6180X time-of-flight sensor and an MLX90614-BCC infrared temperature sensor, respectively. Electrical current and voltage supplied to the SMA wire were monitored using an ACS712 Hall-effect current sensor and a resistive voltage-divider module.

Actuation of the SMA wire was controlled via a logic-level N-channel MOSFET driven by a PWM signal generated by the microcontroller, enabling precise regulation of heating power [52]. Power distribution and signal routing were implemented using a breadboard and terminal connections, with all sensor and power grounds tied to a common ground node connected to the Arduino to minimize electrical noise. Communication with the host computer was achieved through a USB serial interface, which was used for both program upload and real-time data streaming. The measured signals were continuously logged in CSV format for subsequent analysis. A schematic overview of the complete hardware wiring and system integration is provided in Fig. 4, illustrating the interconnection of the control unit, sensors, power electronics, and SMA actuator.

All sensor measurements, including temperature, displacement, force, current, and voltage, were synchronously transmitted from the Arduino Mega 2560 to a host computer via a USB serial interface. Data were streamed in comma-separated-value (CSV) format and logged in real time using Microsoft Excel, with a fixed sampling interval of 100 ms to ensure temporal alignment across all sensing channels during both heating and cooling phases. The recorded datasets were subsequently used for post-processing, visualization, and analysis of the thermo-electro-mechanical response of the SMA actuator.

Calibration and validation

To ensure the accuracy and reliability of the thermo-electro-mechanical measurements obtained from the SMA actuation system, all sensing channels were calibrated and independently validated using external reference instruments. Electrical current and voltage measurements were verified using calibrated digital multimeters, including a clamp-type multimeter for non-invasive current measurement and a probe-based multimeter for direct voltage verification. The reference readings were compared with the outputs of the ACS712 current sensor and the voltage-divider module to confirm measurement linearity and consistency across the tested operating range.

Temperature measurements acquired from the MLX90614-BCC non-contact infrared sensor were validated using a contact-based digital multimeter equipped with a K-type thermocouple placed directly on the SMA wire surface during controlled heating cycles. Displacement measurements from the VL6180X time-of-flight sensor were validated through independent optical observation using a high-magnification digital inspection microscope in conjunction with a millimeter-scale reference. The close agreement between the external reference instruments and the embedded sensor outputs confirmed the accuracy, repeatability, and robustness of the measurement system employed in this study.

The calibration procedures, measurement performance, and validation characteristics of the sensing modules are summarized in Table 6. The associated measurement uncertainties and the measures adopted to minimize their influence are discussed subsequently.

Sensor drift and response delay were considered negligible during the relatively short experimental duration because all measurements were conducted under stable laboratory conditions and within the

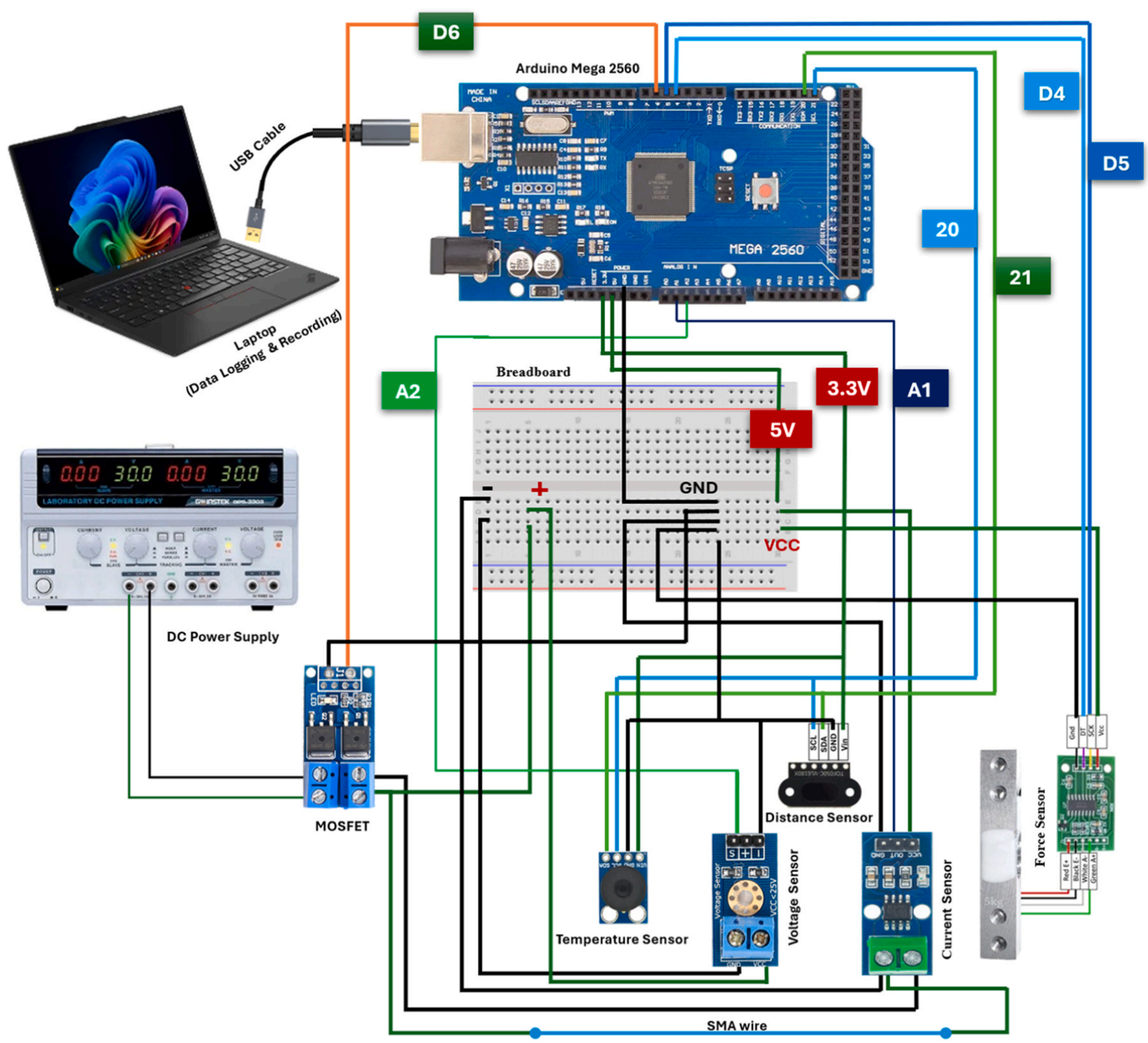

Fig. 4. Wiring diagram of the arduino-based SMA actuation system.

Table 6
Calibration summary and measurement performance of the sensing modules.

Sensor	Reference Instrument	Range	Resolution	Accuracy	Validation Method
MLX90614 IR sensor	K-type thermocouple	20–100 °C	0.02 °C	±0.5 °C	Point-by-point comparison
ACS712 current sensor	Digital multimeter	0–5 A	66–185 mV/A	±1.5%	Current comparison
Voltage sensor	Digital multimeter	0–25 V	Arduino ADC	Validated against digital multimeter	Voltage comparison
Load cell + HX711	Standard weights	0–5 kg	24-bit ADC	0.05% FS	Linear calibration
VL6180X	Digital microscope	0–20 mm	1 mm	±1 mm	Distance comparison

Note: Sensor resolutions and accuracy specifications are based on the respective manufacturers' datasheets, whereas the validation methods correspond to the experimental calibration procedures performed in this study.

specified operating limits of the sensing modules. The overall measurement uncertainty arises primarily from sensor resolution, calibration error, electrical noise, infrared emissivity variation, environmental temperature fluctuations, and sensor alignment during the experimental measurements. Consequently, the remaining measurement uncertainty is not expected to alter the observed thermo-electro-mechanical trends or affect the identification of the proposed operating conditions.

Statistical analysis

The experiments were repeated under each operating condition to evaluate the repeatability and reliability of the proposed thermo-electro-mechanical characterization platform. The measured temperature, force, displacement, current, and voltage data were analyzed using descriptive statistical methods. The quantitative electrical results are reported as mean ± standard deviation (SD), while the corresponding thermo-mechanical performance indicators are summarized in Table 7.

Results and discussion

Non-contact temperature response

Fig. 5 presents the infrared sensor–measured temperature profiles of the 300 mm Flexinol® SMA wire subjected to different current

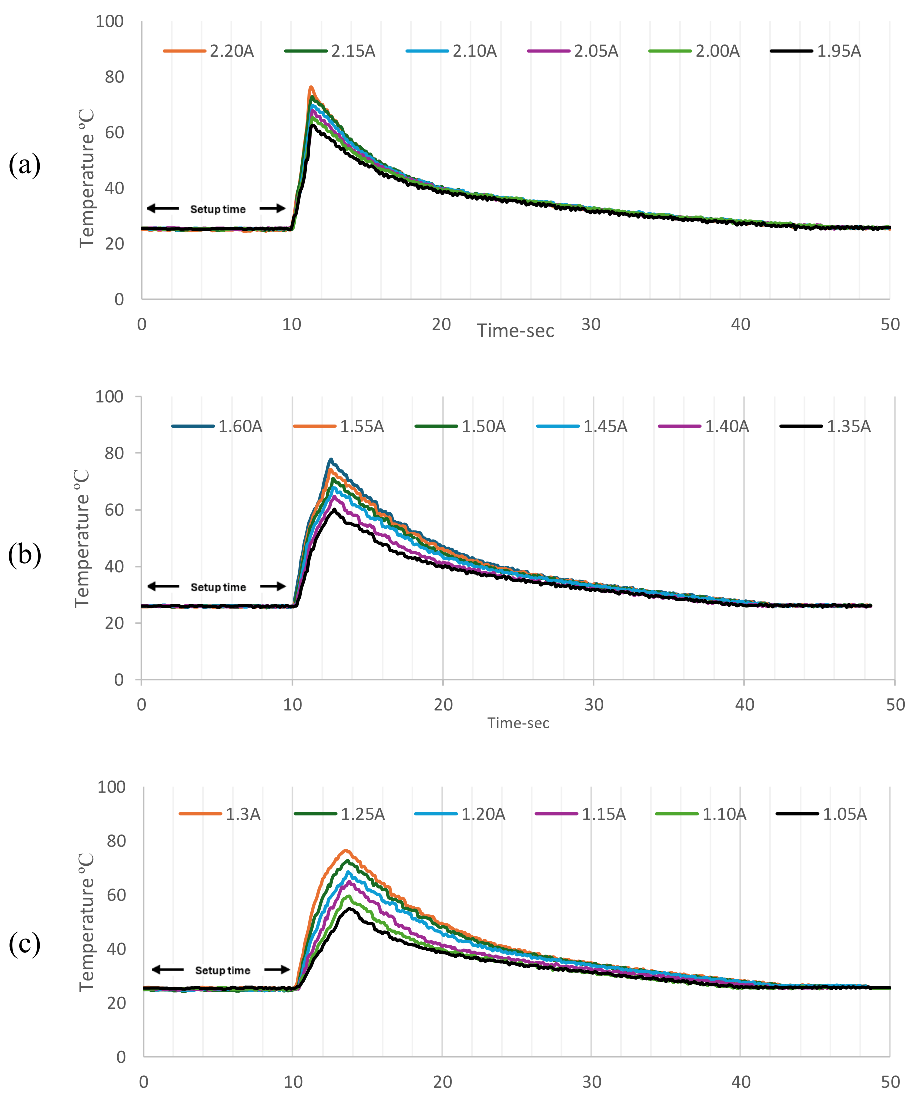

Fig. 5. IR sensor–measured temperature profiles of the 300 mm SMA wire for (a) 1 s, (b) 2 s, and (c) 3 s heating durations.

amplitudes and heating durations (1 s, 2 s, and 3 s). For all actuation conditions, the temperature increased sharply immediately after current application, indicating rapid Joule heating and the onset of the martensite-to-austenite phase transformation. The peak temperature showed a clear dependence on both current magnitude and heating duration, confirming the expected Joule heating relationship $Q = I^2Rt$.

For short, high-current pulses (1 s, 1.95–2.20 A), the SMA wire reached the highest peak temperatures (≈ 60–85 °C), enabling fast actuation response suitable for rapid motion tasks. However, these conditions also resulted in steep thermal gradients, which may increase thermal stress and reduce long-term actuator durability. Intermediate heating conditions (2 s, 1.35–1.60 A) produced moderate peak temperatures (≈ 55–80 °C), offering a balanced compromise between actuation speed and thermal safety. Longer heating durations at lower current levels (3 s, 1.05–1.30 A) resulted in controlled temperature rises (≈ 50–75 °C), which are advantageous for repetitive or continuous operation where reduced fatigue and thermal accumulation are critical.

During the cooling phase, all temperature curves exhibited a rapid initial drop followed by a slower decay, consistent with Newtonian convective cooling dominated by natural convection to ambient air. The similarity of the cooling slopes across different current levels suggests that heat dissipation was primarily governed by environmental conditions rather than the initial heating amplitude. This behavior highlights the importance of optimizing heating profiles rather than relying solely on passive cooling for cycle-time reduction [61].

It should be noted that the surface temperatures measured by the MLX90614-BCC infrared sensor are slightly lower than the internal core temperatures of the SMA wire. This offset arises because infrared sensing captures surface radiation, while resistive heating is most intense within the wire core. Previous studies have reported similar discrepancies, with IR-based surface measurements underestimating internal transformation temperatures by approximately 3–8 °C, depending on wire diameter and airflow conditions. Despite this limitation, the IR measurements reliably captured relative temperature trends and transformation behavior [61,62].

Overall, the temperature results demonstrate a clear and reproducible correlation between electrical input parameters and thermal response, validating the selected actuation currents and durations. These findings establish a safe and effective thermal operating window near the austenite-finish temperature (≈ 60–70 °C) and provide a robust basis for subsequent displacement and force characterization, as well as for defining PWM-based control strategies that balance response speed, thermal safety, and actuator longevity.

(a)

(b)

(c)

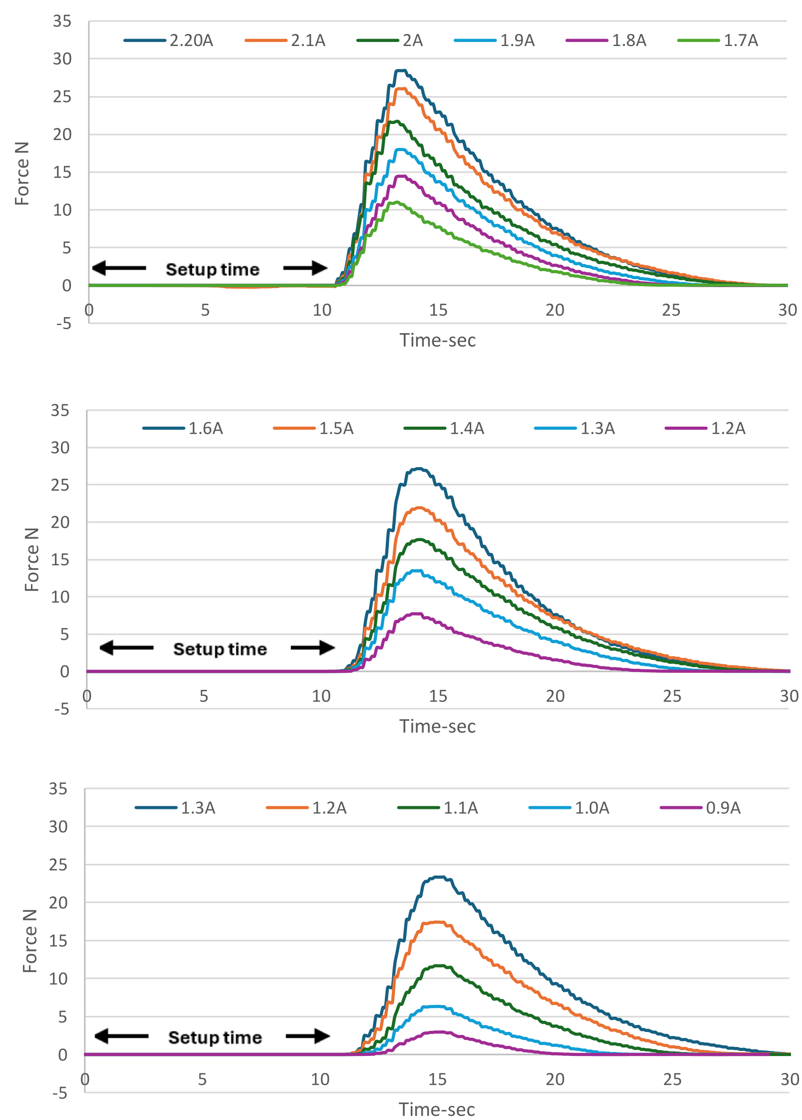

Fig. 6. Force–time response of the 300 mm SMA wire measured by the load cell during (a) 1 s, (b) 2 s, and (c) 3 s heating durations.

Force–time response

Fig. 6 illustrates the force–time responses of the 300 mm SMA wire under different current amplitudes and heating durations (1 s, 2 s, and 3 s), as measured by the load cell. In all cases, force generation commenced immediately after current application, reflecting the rapid martensite-to-austenite phase transformation and the recovery of the pre-strained SMA wire. The force increased sharply during the heating phase and reached a distinct peak before decaying during cooling, indicating reversible thermo-mechanical actuation behavior.

The peak force exhibited a clear dependence on both current magnitude and heating duration. Short, high-current actuation (1 s, ≈ 1.95–2.20 A) produced the highest force outputs, reaching approximately 25–32 N, due to rapid temperature rise and high transformation driving energy. Intermediate actuation conditions (2 s, ≈ 1.35–1.60 A) generated moderate peak forces in the range of 20–28 N, providing a balance between force magnitude and actuation stability. Longer heating durations at lower current levels (3 s, ≈ 1.05–1.30 A) resulted in lower peak forces of approximately 15–22 N, corresponding to slower thermal input and partial transformation. These trends are consistent with the Joule heating relationship $Q = I^2Rt$, confirming that the total actuation energy governs force output.

During the cooling phase, all force profiles displayed a rapid initial decrease followed by a gradual relaxation tail, corresponding to the reverse austenite-to-martensite transformation and the release of stored elastic energy. The similarity of the force decay slopes across different actuation conditions suggests that recovery dynamics were primarily limited by thermal dissipation rather than mechanical resistance. This behavior mirrors the temperature cooling profiles and highlights the strong coupling between thermal and mechanical responses.

From an application perspective, the results indicate that short, high-current pulses are suitable for rapid force generation but may impose higher mechanical and thermal stresses, potentially accelerating material fatigue. In contrast, longer-duration, lower-current actuation provides smoother force evolution with reduced stress, making it more favorable for repetitive or continuous operation. Intermediate actuation conditions offer a compromise between force magnitude, response speed, and operational stability.

Overall, the force measurements demonstrate a strong and reproducible correlation between electrical input, thermal response, and mechanical output. These findings provide a quantitative basis for selecting optimal current–time combinations in PWM-controlled SMA systems, enabling efficient force generation within safe operating limits while enhancing actuator reliability and lifespan.

(a)
(b)
(c)

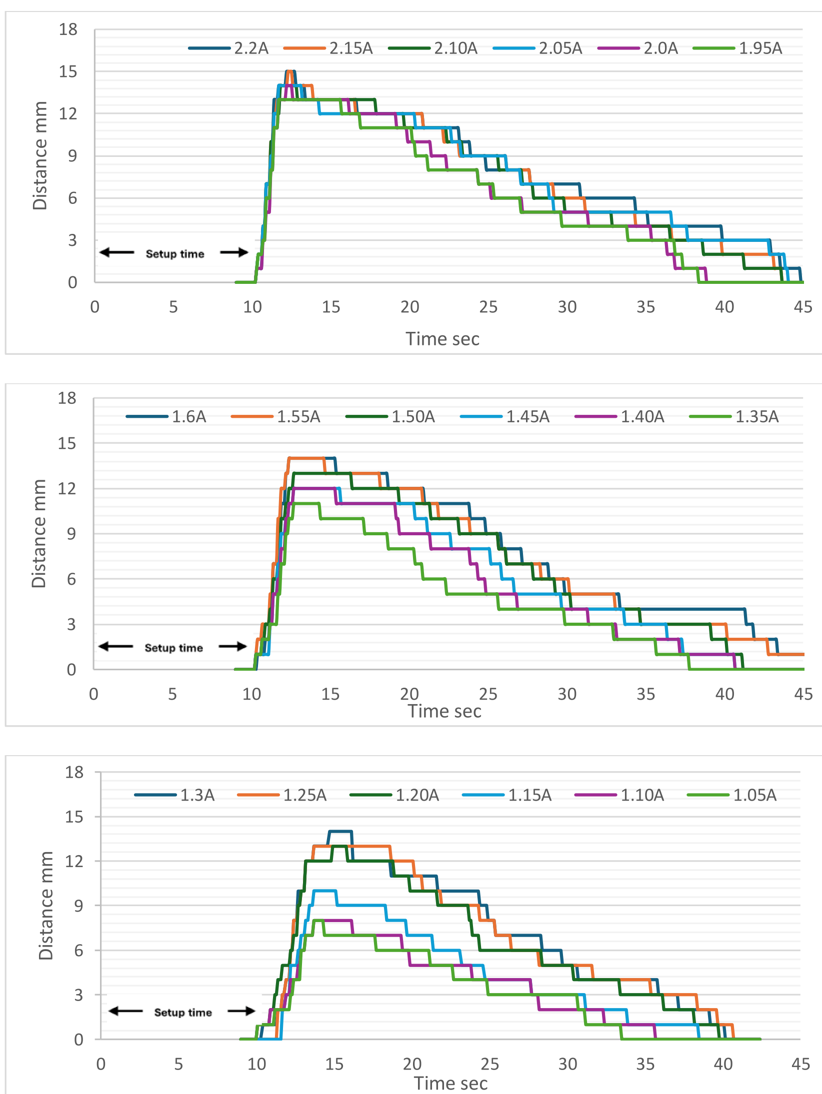

Fig. 7. Displacement–time curve of the 300 mm SMA wire recorded by the VL6180X sensor for different heating durations (a) 1 s, (b) 2 s, and (c) 3 s.

Displacement–time response

Fig. 7 shows the displacement–time responses of the 300 mm SMA wire measured using the VL6180X time-of-flight sensor under different current amplitudes and heating durations (1 s, 2 s, and 3 s). For all actuation conditions, displacement increased rapidly immediately after current application, reflecting the onset of the martensite-to-austenite phase transformation and the associated axial contraction of the SMA wire. The displacement reached its maximum near the end of the heating interval and subsequently decreased during cooling as the material reverted to the martensitic phase.

For short-duration heating (1 s), higher current levels (≈ 2.0–2.2 A) produced the largest contraction strokes, reaching peak displacements of approximately 14–15 mm. This behavior indicates that rapid energy input promotes fast and near-complete phase transformation, resulting in high actuation amplitude. Under intermediate heating conditions (2 s), moderate current levels (≈ 1.35–1.60 A) achieved comparable displacement magnitudes (≈ 12–15 mm) but with smoother transitions and slightly slower recovery, suggesting that extended heating compensates for lower current by sustaining the transformation energy. For longer heating durations (3 s), lower current levels (≈ 1.05–1.25 A) still produced measurable contraction (≈ 10–13 mm), accompanied by more gradual displacement evolution and extended cooling times due to reduced thermal gradients and slower heat dissipation.

Across all tests, the displacement–time profiles exhibited a characteristic heating plateau followed by a gradual decay during cooling, consistent with the hysteretic thermo-mechanical behavior of NiTi SMA materials. The displacement magnitude scaled with the total thermal energy input, in agreement with the Joule heating relationship $Q = I^2Rt$, confirming that both current amplitude and heating duration govern the effective actuation stroke. In contrast, the similarity of the cooling slopes across different conditions indicates that recovery dynamics were dominated by convective heat loss to the ambient environment rather than electrical parameters.

From a functional perspective, short, high-current pulses enable rapid and large displacements but introduce more abrupt motion, which may increase mechanical stress and fatigue. Longer heating durations at lower currents yield smoother, more stable actuation with improved reversibility, making them more suitable for repetitive or rehabilitation-oriented applications. Overall, the displacement results demonstrate a strong coupling between electrical input, thermal response, and mechanical output, providing essential guidance for optimizing PWM-based control strategies that balance actuation speed, stroke magnitude, and long-term reliability.

Current and voltage responses

The electrical behavior of the SMA actuator was evaluated through

(a)
(b)
(c)

Fig. 8. Current–time response of the 300 mm SMA wire for different heating durations (a) 1 s, (b) 2 s, and (c) 3 s.

synchronized current–time and voltage–time measurements, as presented in Fig. 8 and Fig. 9, respectively. The current–time profiles recorded using the ACS712 sensor (Fig. 8) exhibit well-defined, flat plateaus during the heating intervals for all tested actuation durations (1 s, 2 s, and 3 s), confirming stable and regulated current delivery throughout each activation cycle. Each pulse is characterized by a rapid rise upon MOSFET switching, a steady-state region with minimal fluctuation, and an abrupt drop to zero at switch-off, demonstrating precise timing control and reliable PWM-based actuation. The absence of overshoot, drift, or transient instability across repeated cycles highlights the robustness of the electrical control circuit and indicates that temperature-induced resistance variations of the NiTi wire did not significantly disturb current regulation within the selected operating range.

The corresponding voltage–time responses shown in Fig. 9 further confirm the electrical stability of the system. The measured voltage plateaus closely follow the rectangular switching profile of the MOSFET and fall within the theoretical voltage ranges predicted by Ohm's law, based on the calculated electrical resistance of the 300 mm SMA wire (≈ 2.49 Ω). These theoretical voltage bands, summarized in Table 2, are in strong agreement with the experimentally observed values for high-, mid-, and low-current actuation regimes, confirming accurate and repeatable energy delivery. Minor voltage variations observed along the plateau are expected and can be attributed to temperature-dependent changes in the electrical resistivity of NiTi during martensite–austenite phase transformation, a phenomenon well documented in SMA literature.

Taken together, Figs. 8 and 9 demonstrate that the SMA actuator operated under tightly controlled and repeatable electrical conditions. The strong agreement between measured current, measured voltage, and theoretical predictions confirms that the applied Joule heating energy $Q = I^2Rt$was both predictable and consistent. This electrical stability directly underpins the thermal, force, and displacement responses discussed in the preceding sections, validating the Arduino-based PWM control platform as a reliable foundation for electrical optimization and future multi-channel SMA actuation in rehabilitation-oriented applications.

Quantitative performance analysis

To complement the time-history responses presented in Figs. 5–9, the principal thermo-electro-mechanical performance indicators extracted from the experimental measurements are summarized in Table 7. These quantitative metrics provide a concise comparison of the three operating conditions and facilitate quantitative evaluation of the electrical input, thermal response, and mechanical output of the SMA actuator for wearable rehabilitation applications.Table 8

As summarized in Table 7, all three operating conditions produced

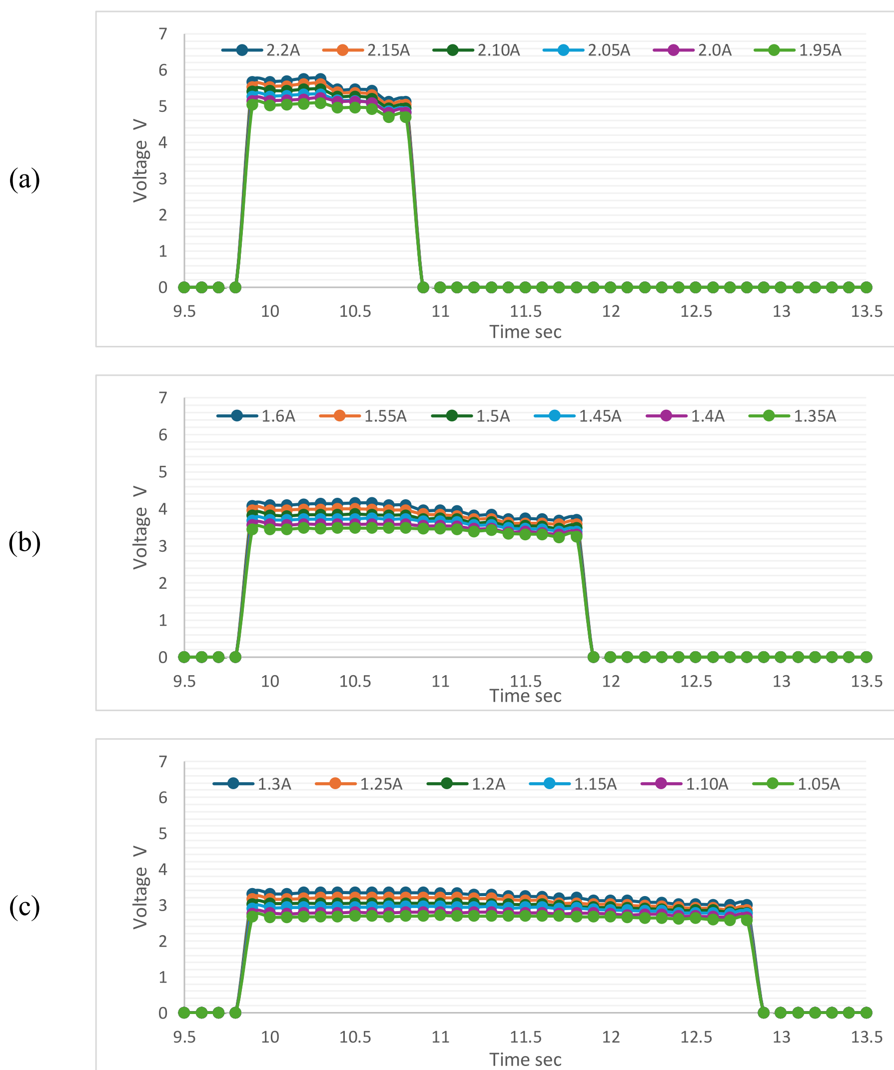

Fig. 9. Voltage–time response of the 300 mm SMA wire for different heating durations (a) 1 s, (b) 2 s, and (c) 3 s.

Table 7
Theoretical voltage ranges of the 300 mm SMA wire based on Ohm's law.

Heating Condition	Current Range (A)	Expected Voltage Range (V)
High-current set −1 s	$I = 2.20$to 1.95 A	$V \approx 5.48$to 4.86 V.
Mid-current set −2 s	$I = 1.60$to 1.35 A	$V \approx 3.98$to 3.36 V.
Low-current set −3 s	$I = 1.30$to 1.05 A	$V \approx 3.24$to 2.61 V.

comparable peak temperatures ranging from 76.30 to 77.84 °C, indicating that each operating condition successfully reached the austenitic transformation range required for SMA activation. The highest mechanical output was obtained under the 2.2 A–1 s condition, which generated a peak force of 28.40 N and a maximum displacement of 15 mm. Reducing the current while proportionally increasing the heating duration gradually decreased the peak force, whereas the peak displacement remained nearly unchanged (14–15 mm), demonstrating that comparable actuation strokes can be achieved with lower electrical power when a longer activation period is permitted. The mean electrical power decreased from 12.35 W to 4.18 W as the applied current decreased from 2.2 A to 1.3 A. Nevertheless, the total electrical energy supplied during each operating condition remained nearly constant (12.35–12.73 J), indicating that the different current-duration combinations primarily modified the heating rate and transient thermo-mechanical response rather than the overall energy input. These findings provide practical operating guidelines for selecting suitable electrical actuation conditions according to the response speed and force requirements of wearable rehabilitation systems.

Beyond the quantitative performance evaluation, the practical implications of the proposed characterization platform for wearable rehabilitation applications and future control development are discussed in the following sections.

Applicability to wearable rehabilitation systems

Although the present experiments were conducted using a single Flexinol® SMA wire under controlled laboratory conditions, the objective of this study was to establish the thermo-electro-mechanical characteristics of the actuator before integration into wearable rehabilitation devices. This characterization approach is commonly adopted in the development of SMA-driven rehabilitation systems, since the actuator's performance directly determines the achievable force, displacement, response time, and thermal behavior of the final wearable device. The extracted performance indicators therefore provide practical design guidelines for actuator selection and operating-condition optimization in future SMA-based rehabilitation gloves. This actuator-level characterization approach has also been employed in the development of the proposed W-DFAS rehabilitation glove, where the experimentally characterized SMA actuator served as the foundation for the complete wearable rehabilitation system [28].

Future control strategies

The proposed characterization platform also provides a suitable experimental foundation for the development of advanced closed-loop control strategies for SMA actuators. By simultaneously acquiring temperature, force, displacement, current, and voltage in real time, the platform generates synchronized multi-sensor datasets that can be used for controller design, parameter identification, and performance optimization. Unlike open-loop current excitation, the measured feedback signals provide the sensing and data acquisition framework required for future implementation of intelligent control approaches, including adaptive control, fuzzy logic control, model predictive control (MPC), and machine learning-based control algorithms to improve motion accuracy, response speed, thermal safety, and robustness against actuator nonlinearities. Recent developments in intelligent actuator control, including adaptive RISE control, reinforcement learning, and model-data hybrid control strategies developed for electrohydraulic systems, demonstrate the effectiveness of combining model knowledge with experimental data for nonlinear control and optimization. Although these intelligent control strategies were originally developed for hydraulic and electrohydraulic actuators, they provide valuable inspiration for future SMA control through adaptive learning, reinforcement learning, and model-data hybrid optimization, particularly when combined with synchronized thermo-electro-mechanical datasets generated by the proposed characterization platform. Furthermore, the automatic data logging capability facilitates the development of data-driven models and digital twins for future wearable rehabilitation systems. Therefore, the proposed platform serves not only as a thermo-electro-mechanical characterization system but also as an experimental testbed for future intelligent control development and wearable rehabilitation research. [66–72].

Conclusion

This study presented a comprehensive experimental investigation of a 300 mm NiTi shape-memory-alloy (SMA) wire actuator under controlled electrical excitation, with synchronized measurement of thermal, mechanical, and electrical responses. A fully integrated Arduino-based control and data-acquisition platform was successfully developed, enabling precise regulation of current, pulse duration, and real-time monitoring of temperature, force, displacement, voltage, and current during actuation cycles.

The results demonstrated a strong and consistent coupling between electrical input energy and actuator performance. Current–time and voltage–time measurements confirmed stable, repeatable, and well-regulated electrical excitation, with measured voltage plateaus closely matching theoretical values predicted by Ohm's law. This agreement verified accurate Joule heating delivery and confirmed the reliability of the PWM-controlled MOSFET actuation circuit. Minor voltage variations observed during heating were attributed to the temperature-dependent resistivity of NiTi during martensite–austenite phase transformation and remained within safe operating limits.

Thermal analysis using the MLX90614-BCC infrared sensor revealed predictable temperature evolution under different current–time combinations. Short, high-current pulses generated rapid temperature rise suitable for fast actuation, while longer, lower-current pulses produced smoother heating profiles advantageous for fatigue reduction and long-term operation. The measured surface temperatures remained within the effective transformation range of the SMA wire, validating the selected actuation window for safe operation.

Force and displacement measurements further confirmed that actuator output scales with thermal energy input. Higher currents produced larger and faster force and displacement responses, whereas longer heating durations improved motion smoothness and recovery stability.

Table 8
Quantitative thermo-electro-mechanical performance indicators of the SMA actuator under different current-duration operating conditions.

Current (A)	Time (s)	Peak Temp. (°C)	Peak Force (N)	Peak Displacement (mm)	Mean Voltage ± SD (V)	Mean Current ± SD (A)	Mean Power (W)	Energy (J)
2.2	**1**	**76.30**	**28.40**	**15**	**5.524 ± 0.240**	**2.236 ± 0.051**	**12.35**	**12.35**
1.6	**2**	**77.84**	**27.15**	**14**	**3.967 ± 0.178**	**1.605 ± 0.035**	**6.37**	**12.73**
1.3	**3**	**76.34**	**23.30**	**14**	**3.217 ± 0.128**	**1.300 ± 0.046**	**4.18**	**12.55**

These findings highlight an important trade-off between rapid response and mechanical stress, which is particularly relevant for rehabilitation applications requiring both dynamic and gentle motion profiles.

Overall, the experimental results confirm that controlled combinations of current amplitude and heating duration provide a flexible means of tuning SMA actuator behavior. The validated experimental platform establishes a reliable foundation for PWM-based optimization, cyclic durability studies, and extension toward multi-channel SMA actuation. These outcomes directly support the future development of wearable and rehabilitation devices, where adaptable force, displacement, and response speed are essential for patient-specific therapy protocols.

Abbreviations

SMA	Shape memory alloy
PWM	Pulse-width modulation
IPMCs	Ionic polymer–metal composites
DEAs	Dielectric elastomers
PEPs	Piezoelectric polymers
MOSFET	Metal–oxide–semiconductor field-effect transistor
LT	Low-transformation-temperature
CSV	Comma-separated-value
ToF	Time-of-flight

.

Authors' contributions

Q. Y. Hamid designed the study, developed the methodology, performed the experiments, and prepared the manuscript. W. Z. Wan Hasan supervised the project, provided resources, and critically revised the manuscript. M. A. Azmah Hanim and A. A. Nuraini supported methodology development, validation, investigation, and technical review. M. N. Hamidon contributed to data interpretation and manuscript review. All authors read and approved of the final manuscript.

Funding

This research was fully funded by the Universiti Putra Malaysia Research Grant (Putra Grant UPM, GP-GPB/2021/9699100).

Declaration of Competing Interest

The authors declare that they have no known competing financial interests or personal relationships that could have appeared to influence the work reported in this paper.

Acknowledgments

The authors would like to thank the University Putra Malaysia for supporting this study.

Data availability

Data will be made available on request.

References

[1] D.K. Soother, J. Daudpoto, B.S. Chowdhry, Challenges for practical applications of shape memory alloy actuators, Mater. Res. Express 7 (7) (2020), https://doi.org/10.1088/2053-1591/aba403.
[2] H. Rodrigue, W. Wang, D.R. Kim, S.H. Ahn, Curved shape memory alloy-based soft actuators and application to soft gripper, Compos. Struct. 176 (2017) 398–406, https://doi.org/10.1016/j.compstruct.2017.05.056.
[3] M. Pan, et al., Soft actuators and robotic devices for rehabilitation and assistance, Adv. Intell. Syst. 4 (4) (2022) 2100140, https://doi.org/10.1002/aisy.202100140.
[4] X. Huang, et al., Highly dynamic shape memory alloy actuator for fast moving soft robots, Adv. Mater. Technol. 4 (4) (2019) 1–9, https://doi.org/10.1002/admt.201800540.
[5] H. Bin, et al., Design and analysis of artificial muscle robotic elbow joint using shape memory alloy actuator, Int. J. Precis. Eng. Manuf. 21 (2) (2020) 249–256, https://doi.org/10.1007/s12541-019-00240-8.
[6] S.S. Mohammed, M. KÖK, I.N. Qader, F. Dağdelen, The developments of piezoelectric materials and shape memory alloys in robotic actuator systems, no. 17, Eur. J. Sci. Technol. (2019) 1014–1030, https://doi.org/10.31590/ejosat.653751.
[7] V. Choyal, S. Khan, P.S.S. Mani, I.A. Palani, P. Singh, Active and passive multicycle actuation characteristics of shape memory alloy-based adaptive composite structures, Smart Mater. Struct. 30 (9) (2021), https://doi.org/10.1088/1361-665X/ac177d.
[8] A. Hallosh Khidhir, Q. Younis Hamid, Ultrasonic attenuation of (Al-SiC) particulate aluminum matrix composite, AL-Rafdain Eng. J. 23 (1) (2015) 30–39, https://doi.org/10.33899/rengj.2015.101024.
[9] Y. She, C. Li, J. Cleary, H.J. Su, Design and fabrication of a soft robotic hand with embedded actuators and sensors, J. Mech. Robot. 7 (2) (2015), https://doi.org/10.1115/1.4029497.
[10] I.I. Gorial, Recent trends in energy-efficient design of mechatronic systems, A Compr. Rev. 25 (1) (2025) 83–98.
[11] S. Rodin, M. Chiodo, A. Corigliano, G. Rota, and C. Maletta, "Fast electrical activation of shape memory alloy spring actuators: sub-second response characterization and performance optimization," pp. 1–20, 2025.
[12] M. Kim, J. Heo, H. Rodrigue, H. Lee, and S. Pané, "Shape Memory Alloy (SMA) Actuators: The Role of Material, Form, and Scaling Effects," vol. 2208517, pp. 1–22, 2023, doi: 10.1002/adma.202208517.
[13] B. He, X. Dong, R. Nie, Y. Wang, S. Ao, G. Wang, Comprehensive shape memory alloys constitutive models for engineering application, Mater. Des. 225 (2023) 111563, https://doi.org/10.1016/j.matdes.2022.111563.
[14] T. Devashena, K. Dhanalakshmi, Simultaneous measurements in shape memory alloy springs to enable structural health monitoring by self-sensing actuation, Arab. J. Sci. Eng. 46 (6) (2021) 6015–6025, https://doi.org/10.1007/s13369-020-05259-y.
[15] Y. Xiong, J. Huang, R. Shu, Thermomechanical performance analysis and experiment of electrothermal shape memory alloy helical spring actuator, Adv. Mech. Eng. 13 (10) (2021) 1–12, https://doi.org/10.1177/16878140211044651.
[16] E. Toptas, M.F. Celebi, S. Ersoy, Measurement of temperature and displacement with niti actuators under certain electrical conditions, J. Meas. Eng. 9 (2) (2021) 87–94, https://doi.org/10.21595/jme.2021.21841.
[17] W.G. Ali Abdelaal, G. Nagib, Modeling and simulation of SMA actuator wire. Proc. 2014 9th IEEE Int. Conf. Comput. Eng. Syst. ICCES 2014, 2014, pp. 401–405, https://doi.org/10.1109/ICCES.2014.7030993.
[18] G.J. Reddy, S. Maniprakash, Influence of various design parameters, vol. 0123456789, strain Recovery Perform. SMA-Embed. smart Actuators (2025). vol. 0123456789.
[19] M. Pan, et al., Soft actuators and robotic devices for rehabilitation and assistance, Adv. Intell. Syst. 4 (4) (2022), https://doi.org/10.1002/aisy.202100140.
[20] R. Britz, P. Motzki, Analysis and evaluation of bundled SMA actuator wires (no. xxxx, p), Sens. Actuators A Phys. (2021) 113233, https://doi.org/10.1016/j.sna.2021.113233.
[21] J. Mohd Jani, M. Leary, A. Subic, M.A. Gibson, A review of shape memory alloy research, applications and opportunities, Mater. Des. 56 (2014) 1078–1113, https://doi.org/10.1016/j.matdes.2013.11.084.
[22] C. Liu, J. Lu, H. Yang, K. Guo, Current state of robotics in hand rehabilitation after stroke: a systematic review, Appl. Sci. 12 (9) (2022), https://doi.org/10.3390/app12094540.
[23] Q.Y. Hamid, W.Z. Wan Hasan, M.A. Azmah Hanim, A.A. Nuraini, M.N. Hamidon, H.R. Ramli, Shape memory alloys actuated upper limb devices: a review, Jun. 01, in: Sensors and Actuators Reports, 5, Elsevier B.V., 2023, https://doi.org/10.1016/j.snr.2023.100160.
[24] B.S. Shariat, et al., Functionally graded shape memory alloys: design, fabrication and experimental evaluation, Mater. Des. 124 (2017) 225–237, https://doi.org/10.1016/j.matdes.2017.03.069.
[25] J. Arias Guadalupe, D. Copaci, D. Serrano Del Cerro, L. Moreno, D. Blanco, Efficiency analysis of SMA-based actuators: possibilities of configuration according to the application, Actuators 10 (3) (2021) 1–19, https://doi.org/10.3390/act10030063.
[26] DYNALLOY inc., "Technical characteristics of FLEXINOL ® Actuator Wires Table of Contents Makers of Dynamic Alloys NICKEL - TITANIUM ALLOY PHYSICAL PROPERTIES," pp. 1–12, 2013.
[27] N. Vasudha, K. Uma Rao, Shape memory alloy properties, modelling aspects and potential applications - a review, J. Phys. Conf. Ser. 1706 (1) (2020), https://doi.org/10.1088/1742-6596/1706/1/012190.
[28] Q.Y. Hamid, W.Z.W. Hasan, M.A.A. Hanim, A.A. Nuraini, M.N. Hamidon, W-DFAS rehabilitation glove: design and experimental validation (no. May), Eng. Sci. Technol. Int. J. 79 (2026) (no. May).
[29] D. Copaci, L. Moreno, D. Blanco, Two-stage shape memory alloy identification based on the Hammerstein–Wiener model (no. September), Front. Robot. AI 6 (2019) 1–10, https://doi.org/10.3389/frobt.2019.00083.
[30] J.A. Guadalupe, D. Copaci, P.M. Navarro, L. Moreno, and D. Blanco, "Mechatronics A novel multi-wire SMA-based actuator with high-frequency," vol. 91, no. February, 2023.
[31] A. Hadi, K. Alipour, S. Kazeminasab, A. Amerinatanzi, M. Elahinia, Design and prototyping of a wearable assistive tool for hand rehabilitation using shape memory alloys, in: In Proceedings of the ASME 2016 Conference on Smart Materials, Adaptive Structures and Intelligent Systems (SMASIS2016), September 28–30, 2016, ASME, *Stowe, VT, USA*, 2016, pp. *1–7*, in: https://asmedigitalcollec

tion.asme.org/SMASIS/proceedings-abstract/SMASIS2016/285418 ([Online]. Available).
[32] E.A. Aner, O.M. Shehata, M. Ibrahim, A. Nancy, A decade of soft robotic manipulators, Adv. Des. Model. Control. Emerg. Chall. (2025).
[33] Z. Shami, T. Arslan, P. Lomax, Wearable soft robots: case study of using shape memory alloys in rehabilitation, Bioengineering 12 (3) (2025) 1–31, https://doi.org/10.3390/bioengineering12030276.
[34] Afzal Khan, Characterization and application of shape memory alloy wires for micro and meso positioning systems," *Georg. Washingt, . 2008. 3324402.*,, Univ. ProQuest Diss. Publ, 2008.
[35] D. Copaci, D. Blanco, L.E. Moreno, Flexible shape-memory alloy-based actuator: mechanical design optimization according to application, Actuators 8 (3) (2019), https://doi.org/10.3390/ACT8030063.
[36] Y. Zhang, X. Xu, Transformation temperature predictions through computational intelligence for NiTi-based shape memory alloys, Shape Mem. Superelasticity 6 (4) (2020) 374–386, https://doi.org/10.1007/s40830-020-00303-0.
[37] A. Czechowicz, S. Langbein, Shape Mem. Alloy. Valves (2015), https://doi.org/10.1007/978-3-319-19081-5.
[38] S. Kazeminasab, A. Hadi, K. Alipour, M. Elahinia, Force and motion control of a tendon-driven hand exoskeleton actuated by shape memory alloys, Ind. Rob. 45 (5) (2018) 623–633, https://doi.org/10.1108/IR-01-2018-0020.
[39] R. Dauksher, Z. Patterson, C. Majidi, Characterization and analysis of a flexural shape memory alloy actuator, Actuators 10 (8) (2021), https://doi.org/10.3390/act10080202.
[40] G.K. Tshikwand, L. Seigner, F. Wendler, M. Kohl, Coupled finite element simulation of shape memory bending microactuator, Shape Mem. Superelasticity 8 (4) (2022) 373–393, https://doi.org/10.1007/s40830-022-00396-9.
[41] H. Zhou, N. Ma, Modeling and experimental implementation of a flexible SMA wire-based gripper for confined space operation, J. Intell. Mater. Syst. Struct. 33 (17) (2022) 2161–2175, https://doi.org/10.1177/1045389X221077428.
[42] N. Keshtkar, et al., Systems actuated by shape memory alloys: identification and modeling, Syst. Theory Control. Comput. J. 1 (2) (2021) 12–20, https://doi.org/10.52846/stccj.2021.1.2.20.
[43] S. Szykowny, M.H. Elahinia, Heat transfer analysis of shape memory alloy actuators, Am. Soc. Mech. Eng. Aerosp. Div. AD (2006) 1–8, https://doi.org/10.1115/IMECE2006-13788.
[44] Y. Wang, S. Zheng, Z. Song, J. Pang, J. Li, A coupling dynamic model for studying the physical interaction between a finger exoskeleton and a human finger, IEEE Access. 8 (2020) 125412–125422, https://doi.org/10.1109/ACCESS.2020.3007799.
[45] P. Senthilkumar, M. Umapathy, Use of load generated by a shape memory alloy for its position control with a neural network estimator, J. Vib. Control. 20 (11) (2014) 1707–1717, https://doi.org/10.1177/1077546313481000.
[46] J. Daudpoto, A. Dehghani-Sanij, R. Richardson, A measurement system for shape memory alloy wire actuators, Meas. Control. 48 (9) (2015) 285–288, https://doi.org/10.1177/0020294015595994.
[47] M. Kurzawa, D. Stachowiak, Investigation on thermo-mechanical behavior of shape memory alloy actuator, Arch. Electr. Eng. 66 (4) (2017) 751–760, https://doi.org/10.1515/aee-2017-0057.
[48] A. Hadi, K. Alipour, S. Kazeminasab, M. Elahinia, ASR glove: a wearable glove for hand assistance and rehabilitation using shape memory alloys, J. Intell. Mater. Syst. Struct. 29 (8) (2018) 1575–1585, https://doi.org/10.1177/1045389X17742729.
[49] D. Serrano, D.S. Copaci, L. Moreno, D. Blanco"SMA based wrist exoskeleton for rehabilitation therapy," IEEE Int. Conf. Intell. Robot. Syst., pp. 2318–2323, 2018, doi: 10.1109/IROS.2018.85939872018.
[50] T. Helps, A. Vivek, J. Rossiter, Characterization and Lubrication of Tube-Guided Shape-Memory Alloy Actuators for Smart Textiles, Robotics 8 (94) (2019) 1–13.
[51] P.L. Bishay, et al., Development of a biomimetic transradial prosthetic arm with shape memory alloy muscle wires, Eng. Res. Express 2 (3) (2020) 35041, https://doi.org/10.1088/2631-8695/abb710.
[52] E. Deng, Y. Tadesse, A soft 3d-printed robotic hand actuated by coiled sma, Actuators 10 (1) (2021) 1–24, https://doi.org/10.3390/act10010006.
[53] H. Yahya, D. Laila, A. Haji, A. Majid, S. Karunakaran, and S. Ethaib, "Thermomechanical performance of helical shape memory alloy springs immersed in heated and cooled water system," no. November, 2022.
[54] Q. Xie, et al., Design of a soft bionic elbow exoskeleton based on shape memory alloy spring actuators, Mech. Sci. 14 (1) (2023) 159–170, https://doi.org/10.5194/ms-14-159-2023.
[55] S.M. Lee, J. Park, A soft wearable exoglove for rehabilitation assistance: a novel application of knitted shape-memory alloy as a flexible actuator, Fash. Text. 11 (1) (2024), https://doi.org/10.1186/s40691-024-00377-9.
[56] S. Masiero, A. Celia, G. Rosati, M. Armani, Robotic-assisted rehabilitation of the upper limb after acute stroke, Arch. Phys. Med. Rehabil. 88 (2) (2007) 142–149, https://doi.org/10.1016/j.apmr.2006.10.032.
[57] R.C.V. Loureiro, W.S. Harwin, K. Nagai, M. Johnson, Advances in upper limb stroke rehabilitation: A technology push, Med. Biol. Eng. Comput. 49 (10) (2011) 1103–1118, https://doi.org/10.1007/s11517-011-0797-0.
[58] R. Colombo, et al., Robotic techniques for upper limb evaluation and rehabilitation of stroke patients, IEEE Trans. Neural Syst. Rehabil. Eng. 13 (3) (2005) 311–324, https://doi.org/10.1109/TNSRE.2005.848352.
[59] E.D. Engeberg, S. Dilibal, M. Vatani, J.W. Choi, J. Lavery, Anthropomorphic finger antagonistically actuated by SMA plates, Bioinspiration Biomim. 10 (5) (2015), https://doi.org/10.1088/1748-3190/10/5/056002.
[60] A.J. Theodore, P.L. Bishay, Experimental analysis of fiber-reinforced laminated composite plates with embedded SMA wire actuators, no. November 2021, p, Compos. Struct. 292 (2022) 115678, https://doi.org/10.1016/j.compstruct.2022.115678.
[61] Q. Xie, et al., Design of a SMA-based soft composite structure for wearable rehabilitation gloves (no. March), Front. Neurorobot. 17 (2023), https://doi.org/10.3389/fnbot.2023.1047493.
[62] T. High, C. Pwm, T. Mlx, T. Comfort, and M.A. Conditioning, Single and dual zone IR sensor in TO39 Datasheet General description Features & benefits. [Online]. Available: www.melexis.com/technical-inquiry.
[63] P. Specifications, "YZC-131A load cells manual book, Technical Manual".
[64] U. Guide, "User Guide ACS712 hall current sensor module specifications," pp. 1–1, 2021, [Online]. Available: www.handsontec.com.
[65] N.F. Kamaruzaman, E.J. Abdullah, Design and testing of shape memory alloy actuation mechanism for flapping wing micro unmanned aerial vehicles, IOP Conf. Ser. Mater. Sci. Eng. 270 (1) (2017), https://doi.org/10.1088/1757-899X/270/1/012017.
[66] Z. Yao, X. Liang, S. Wang, J. Yao, Model-data hybrid driven control of hydraulic euler – lagrange systems, IEEE/ASME Trans. Mechatron. 30 (1) (2025) 131–143, https://doi.org/10.1109/TMECH.2024.3390129.
[67] Z. Yao, F. Xu, G. Jiang, S. Member, J. Yao, Data-driven control of hydraulic manipulators by reinforcement learning, IEEE/ASME Trans. Mechatron. 29 (4) (2024) 2673–2684, https://doi.org/10.1109/TMECH.2023.3336070.
[68] Z. Yao, X. Liang, G. Jiang, S. Member, J. Yao, Model-based reinforcement learning control of electrohydraulic position servo systems, IEEE/ASME Trans. Mechatron. 28 (3) (2023) 1446–1455, https://doi.org/10.1109/TMECH.2022.3219115.
[69] Z. Yao, J. Yao, W. Sun, Adaptive RISE control of hydraulic systems neural-networks, with multilayer, IEEE Trans. Ind. Electron. 66 (11) (2019) 8638–8647, https://doi.org/10.1109/TIE.2018.2886773.
[70] M.H. Nguyen, H.V. Dao, K.K. Ahn, Adaptive robust position control of electro-hydraulic servo systems with large uncertainties and disturbances, Appl. Sci. (2022).
[71] M. Onder"RISE-based backstepping control design for an electro-hydraulic arm system with parametric uncertainties," vol. 95, no. 10, pp. 2815–2827, 2022.
[72] J. Li, W. Li, X. Du, Research on the characteristics of electro - hydraulic position servo system of RBF neural network under fuzzy rules, no. 0123456789, Sci. Rep. (2024) 1–15, https://doi.org/10.1038/s41598-024-64262-7.